

EFFECTS OF PEM FUEL CELL DEGRADATION ON THE TRANSPORT PROPERTIES OF THE CATHODE CATALYST LAYER

Omid Babaie Rizvandi ^{1*}, Serhat Yesilyurt ²

¹ Mechatronics Program, Sabanci University, Istanbul, Turkey (Corresponding Author)

² Mechatronics Program, Sabanci University, Istanbul, Turkey

ABSTRACT

Durability is a major issue against the commercialization of proton exchange membrane fuel cells (PEMFC). Several mechanisms play an important role on the degradation of the cathode catalyst layer (CCL) by deteriorating the transport properties of reactants in the CCL mainly. A pseudo three-dimensional (P3D), two-phase, and non-isothermal model is used to study the effects of cell degradation on transport properties of the CCL. Accuracy of the model is verified by comparing the polarization curves from the model with the experimental ones reported in the literature. The model is used to investigate the effects of CCL transport properties and agglomerate parameters on cell performance. Results demonstrate that the cell performance is improved for thinner ionomer film around agglomerates, smaller agglomerates, higher exchange current density, lower transport resistance and higher proton conductivity of the CCL. The transport parameters of the CCL are varied to fit the polarization curves to the experimental ones for an accelerated stress test. It is found that the transport resistances increase exponentially with the carbon loss in the CCL.

Keywords: PEMFC, Cell degradation, Performance loss, Catalyst layer transport properties, Agglomerate parameters

NOMENCLATURE

Abbreviations

AST	Accelerated stress test
CCR	Carbon corrosion reaction
CL	Catalyst layer
DEA	Dead-ended anode
DOF	Number of degrees of freedom
ECSA	Electrochemical surface area
Exp	Experiment

GDL	Gas diffusion layer
HOR	Hydrogen oxidation reaction
IP	In-plane
OER	Oxygen evolution reaction
ORR	Oxygen reduction reaction
P3D	Pseudo three-dimensional
PEMFC	Proton exchange membrane fuel cell
Pt	Platinum
RH	Relative humidity
Sim	Simulation
St	Stoichiometric ratio
TP	Through-plane
agg	Agglomerate
man	Manifold
<i>Symbols</i>	
h	Height
J	Current density
p	Pressure
T	Temperature
V	Voltage
w	Width
δ	Thickness
σ	Conductivity

1. INTRODUCTION

Low (zero) emission, high energy density, high efficiency, low operating temperature, and fast startup makes the proton exchange membrane fuel cell (PEMFC) a promising candidate as a power source for stationary and portable applications. However, durability is an important issue weighing against the commercialization of PEMFCs. Various transient in the operation of the PEMFC, including start-up and shut-down, high power, load transients, and idling have a major impact on the performance loss of the PEMFC [1]. The degradation of the cathode catalyst layer (CCL) through carbon

corrosion and platinum dissolution are among the chief mechanisms that contribute to the performance loss through deterioration of the transport properties in the CCL [2].

The formation of the hydrogen-air interface in the anode during transients causes the carbon corrosion reaction in the CCL. Hydrogen-air interface in the anode flow field divides the cell into two parts: an active part that operates normally with hydrogen oxidation reaction (HOR) in the anode and oxygen reduction reaction (ORR) in the cathode; and a passive part without hydrogen in which the current reverses direction with ORR in the anode the carbon corrosion and oxygen evolution reactions (CCR and OER, respectively) in the cathode [3]. The corrosion of the carbon support in the cathode CL results in a drop in the electrochemical surface area (ECSA), loss of the hydrophobicity of the CL, and a lower porosity, which reduces the mass transport of oxygen and liquid water removal [4-6].

Platinum (Pt) is needed in the cathode to improve the sluggish ORR. It has been shown that Pt can dissolve in acidic media at pH values representative of the electrolytes of PEMFCs [7]. Pt solubility increases for smaller particles, especially at high potentials and voltage cycling [8,9]. Pt degradation involves Ostwald-ripening and particle coalescence and detachment [10], which causes loss of ECSA at the CCL [11].

Several studies have been conducted to investigate the effects of the CCR in the CCL on cell performance. Chen et al. [12] developed a one-dimensional isothermal model along the channel to investigate the effects of the dead-ended anode (DEA) operation on the CCR in the CCL. The authors included reduction of the ECSA via a power law relation based on the ratio of the remaining carbon and its initial level. It was found that the CCR induces a non-recoverable open circuit voltage drop due to the loss of the ECSA. Kulikovskiy [13] developed a physical model of the CL performance for the polarization curve prediction to quantify the changes in the model parameters (oxygen diffusivity, proton conductivity, and exchange current density) by adjusting these parameters for the polarization curves fitting before and after the degradation of the cell. According to that study [13], the exchange current density does not change significantly while the oxygen diffusivity and proton conductivity of the cathode CL change dramatically. Baroody et al. [14] developed a physical-statistical model for Pt degradation including dissolution, coagulation, detachment, and re-deposition. The variations of ECSA, particle size distribution (PSD), Pt mass distribution, and CL thickness were

predicted simultaneously. Dhanushkodi et al. [15] developed a CCR kinetic model to evaluate the carbon loss during accelerated stress tests (AST). The authors suggested an exponential relation for the performance losses as a function of the carbon loss.

In this paper, we used a two-phase, non-isothermal and pseudo-3D model to investigate the effects of the cell degradation on transport properties of the CCL. The model is validated by comparing the polarization curves with the experimental data reported in [16]. Effects of the CL transport properties (resistance against oxygen transport, proton conductivity, and exchange current density of ORR) and agglomerates parameters (ionomer film thickness around the agglomerates and agglomerates radius) on the cell performance are investigated. Moreover, the variations in transport parameters in the CCL with the carbon loss are obtained by fitting the polarization curves to the ones reported in [16] during an AST. To the best of our knowledge, variations of the CCL transport resistances with the carbon loss has not been studied experimentally or numerically.

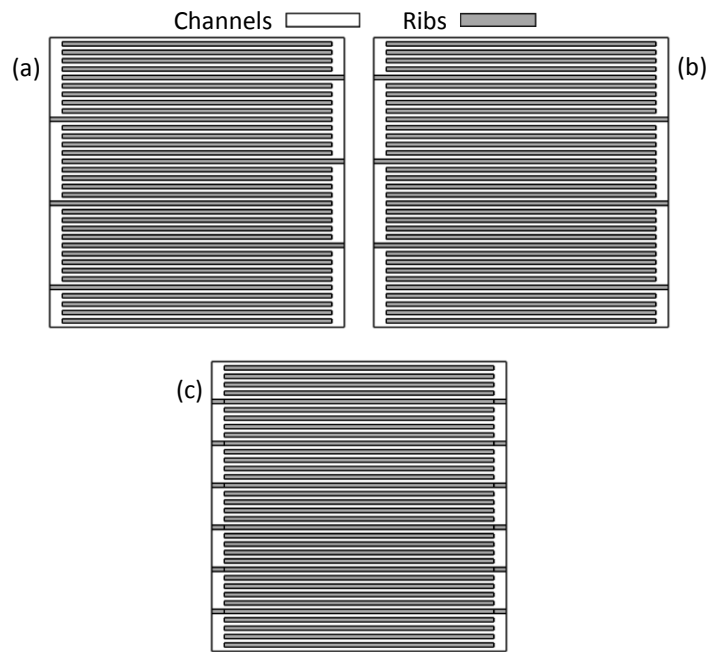


Fig 1 Flow fields for: (a) anode, (b) cathode, and (c) anode and cathode on a single surface which forms the modeling domain; anode and cathode inlets are at top right and left corners, respectively, and anode and cathode outlets are at bottom left and right corners, respectively

2. METHODOLOGY

A P3D model with two-phase and non-isothermal assumptions, [17], is considered for the simulations.

Modified serpentine-channel flow fields with 5-pass channels and manifolds at the sides are used for both anode and cathode flow fields, as shown in Fig. 1. Flow fields are mirror images of each other with an active area of 50 cm². Anode and cathode flow fields are projected on a single surface to form the computational domain, as demonstrated in Fig. 1c.

2.1 Governing equations

A detailed discussion of the governing equations can be found in our previous work [17]. Height-averaged transport equations of mass, momentum, species, liquid water, and energy are solved together over the resulting channels and GDLs. Through-plane (TP) fluxes in the channels and GDLs are represented by reactions. In-plane (IP) transport of the model variables is not considered in the CLs and membrane as they are very thin. CLs are modeled as thin layers resist the transport of the reactants and protons to the active sites. The resistance of the membrane against the dissolved water and proton transport is also considered.

Brinkman equations are used to obtain the velocity field in the channels and GDLs, Maxwell-Stefan equations are used for the transport of the species by diffusion and advection, Butler-Volmer equations are used for the anode HOR, and an agglomerate model is used for the cathode ORR. Distribution and transport of the liquid water in the cathode GDL, dissolved water distribution and transport in the electrolyte phase, and temperature distribution in the channels and GDLs are included in the model as well. Basic model parameters are the same as the ones reported in Table 2 of our previous study [17], and geometric, operation, and model parameters modified for this study are listed in Table 1.

In our previous paper [17], the resistance of the CCL against the oxygen transport was defined based on the CL thickness, porosity, and diffusion coefficient, Eq. (61), and proton conductivity of the CL was defined based on the water content and temperature, Eq. (52). However, constant values are considered for them in this study as the aim is to determine their variations with the cell degradation, and it has been reported in recent studies that those definitions are not accurate enough, as mentioned by Karan [18].

Table 1 Geometric, operation, and model parameters

Parameter	Value	Description
W_{ch}	1×10^{-3} m	Channel width [19]
W_{rib}	1.03×10^{-3} m	Rib width [19]
W_{man}	3×10^{-3} m	Manifold width [19]
h_{ch}	1×10^{-3} m	Channel height [19]

h_{GDL}	2×10^{-4} m	GDL thickness [19]
δ_{CL}	7 and 12×10^{-6} m	Anode and cathode CLs thicknesses [19]
δ_m	18×10^{-6} m	Membrane thickness [19]
T	353 K	Operating temperature [16]
p	2.75 bar	Operating pressure [16]
$RH_{\{an,ca\}}$	1	Anode and cathode inlet relative humidity [16]
$St_{\{an,ca\}}$	1.2 and 2	Anode and cathode flow stoichiometric ratios [16]
$R_{O_2,CL}$	0.1 s m^{-1}	Resistance of the cathode CL against oxygen transport
σ_{CL}	4 S m^{-1}	Proton conductivity of the CL
$\alpha_{\{an,ca\}}$	1	Anodic and cathodic charge transfer coefficients
R_{solid}	$3.5 \times 10^{-6} \Omega \text{ m}^2$	Electric resistance of the cell components
r_{agg}	1×10^{-7} m	Agglomerates radius [20]
δ_i	1×10^{-8} m	Ionomer film thickness around the agglomerates [20]

2.2 Boundary conditions

Inlet boundary conditions are constant flow rates calculated based on the flow stoichiometric ratios, operating temperature, and mass fractions of the species calculated based on the inlet relative humidity (RH) [17]. Outlet boundary conditions are the operating pressure and outflow boundary conditions for the species, water saturation, and temperature [17]. Moreover, no-slip, no-flux, and thermal insulation boundary conditions are applied to the walls of the computational domains.

2.3 Numerical approach

Brinkman, Maxwell-Stefan, Butler-Volmer, water saturation, dissolved water, and energy equations are coupled and solved numerically by the COMSOL Multiphysics software. Quadrangular mesh with linear elements is used to discretize the governing equations. The number of elements and degrees of freedom (DOF) are about 23 and 603.5 K. Fully-coupled solver with Newton iterations and direct MUMPS are used to solve the equations. The runtime of the simulations for each polarization curve is about 3 hours.

3. RESULTS

Accuracy of the model is verified by comparing the polarization curves from the model and the experimental data reported by Spornjak et al. [16]. Figure 2 shows an excellent agreement between the polarization curves for the operation, geometric, and model parameters listed in Tables 1.

In several studies, e.g. [4-6, 11], it has been shown

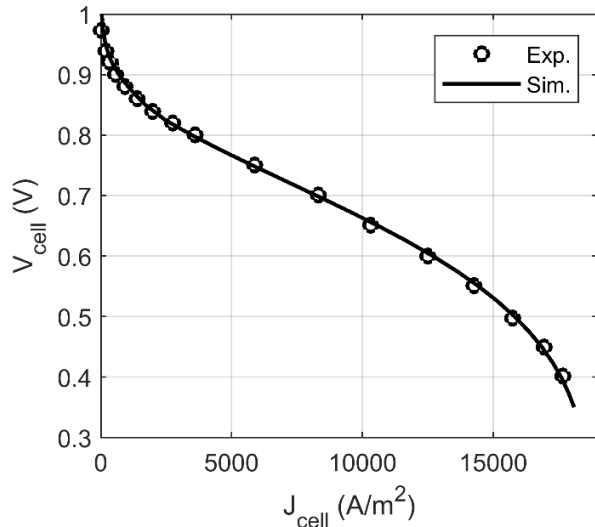


Fig 2 Comparison of the polarization curves from the model and the experimental data reported in [16]

that carbon corrosion and platinum degradations at the CL make changes in the CL resistance against reactants

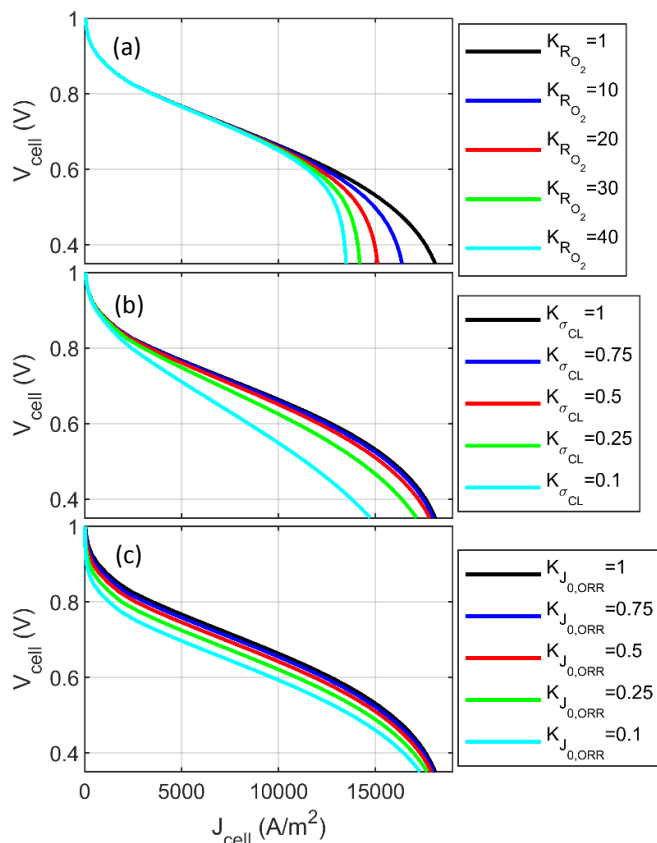


Fig 3 Polarization curves for different: a) resistance of the CL against oxygen transport, b) proton conductivity of the CL, and c) exchange current density of ORR; K is a coefficient that multiplies to these parameters for their variations

transport, conductivity, and reaction kinetics. Figure 3

shows the effects of the CL resistance against oxygen transport, $R_{O_2,CL}$, proton conductivity of the CL, σ_{CL} , and exchange current density of ORR, $J_{0,ORR}$, on the polarization curve (cell performance). It is seen that $R_{O_2,CL}$ has an important effect on the limiting current density, σ_{CL} affects the ohmic part of the polarization curve by varying its slope, and $J_{0,ORR}$ moves the polarization curve downward due to its effect on the cathodic activation overpotential.

In addition to the modifications in the transport properties according to the level of degradation in the CCL, the agglomerate parameters need to be modified as well. For instance, Pokhrel et al. [21] showed the agglomeration of the Pt/C and increase in the thickness of the ionomer film around the agglomerates by X-ray computed tomography of a CL under degradation by an AST. Figure 4 shows the effects of the ionomer film thickness around the agglomerates, δ_i , and the agglomerates radius, r_{agg} , on the polarization curve (cell performance). The limiting current density is reduced for thicker ionomer films due to a longer pass for oxygen diffusion through the ionomer to reach the active sites for the ORR, as indicated in Eq. (59) of [17]. Moreover, the cell performance is dropped for bigger agglomerates, which is because of the effect of the agglomerate radius on the

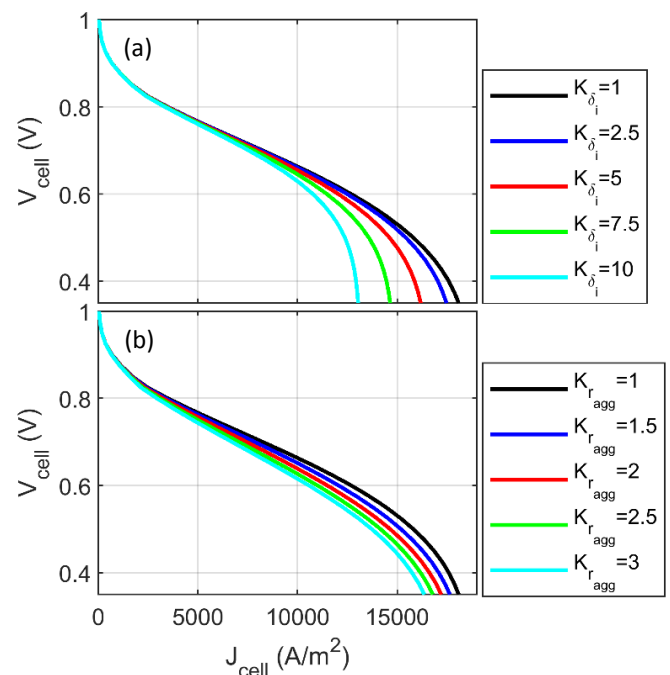


Fig 4 Polarization curves for different: a) ionomer film thickness around the agglomerates, and b) agglomerates radius; K is a coefficient that multiplies to these parameters for their variations

effectiveness factor through changing Thiele modulus, as shown in Table 6 of [17].

Polarization curves from the experiments during an AST, [16], show changes in all parts of the curve, i.e. activation, ohmic, and transportation losses, as shown in Fig. 5. $R_{O_2,CL}$, σ_{CL} , and $J_{O,ORR}$ are varied to capture the changes in the CL transport properties through matching the polarization curves. Agglomerate parameters are not varied here and their effects are considered in $R_{O_2,CL}$ as agglomerate parameters mostly affect the transportation part of the polarization curve, as shown in Fig. 4. Therefore, $R_{O_2,CL}$, σ_{CL} , and $J_{O,ORR}$ are varied to fit the changes in the transportation losses, the slope of the ohmic losses, and activation losses of the polarization curves, respectively. Figure 5 shows the comparisons of the polarization curves from the simulations and the experiments reported in [16] at 0, 3, 4, 5, and 7 h with a very good agreement between them. $R_{O_2,CL}$, σ_{CL} , and $J_{O,ORR}$ are varied to match the polarization curves and plotted versus the carbon loss in the CL in Fig. 6. Interestingly, variations of the transport parameters with the carbon loss are exponential, similar to the behavior reported in [15] for potential losses versus carbon losses.

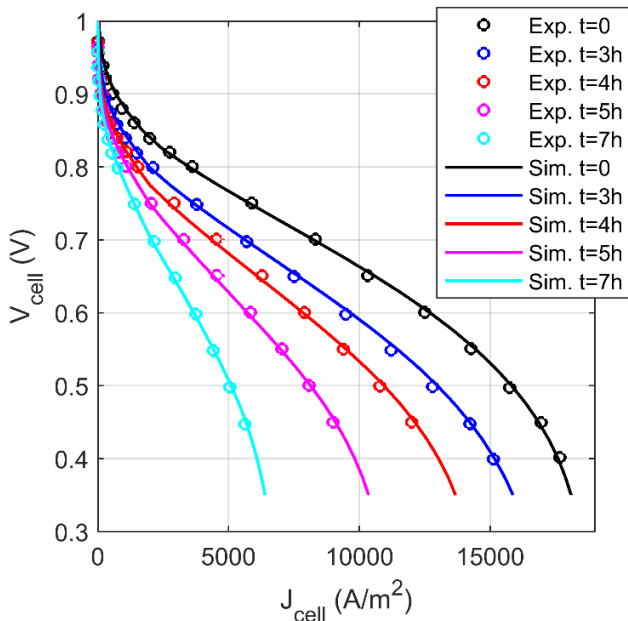


Fig 5 Comparisons of the polarization curves from the model and experiments, [16], at 0, 3, 4, 5, and 7 h

4. CONCLUSIONS

A two-phase and non-isothermal P3D-model is used to study the effects of the cell degradation on transport properties of the cathode CL. The model is validated by comparing the polarization curves with the experimental data reported in [16]. The model is used to investigate

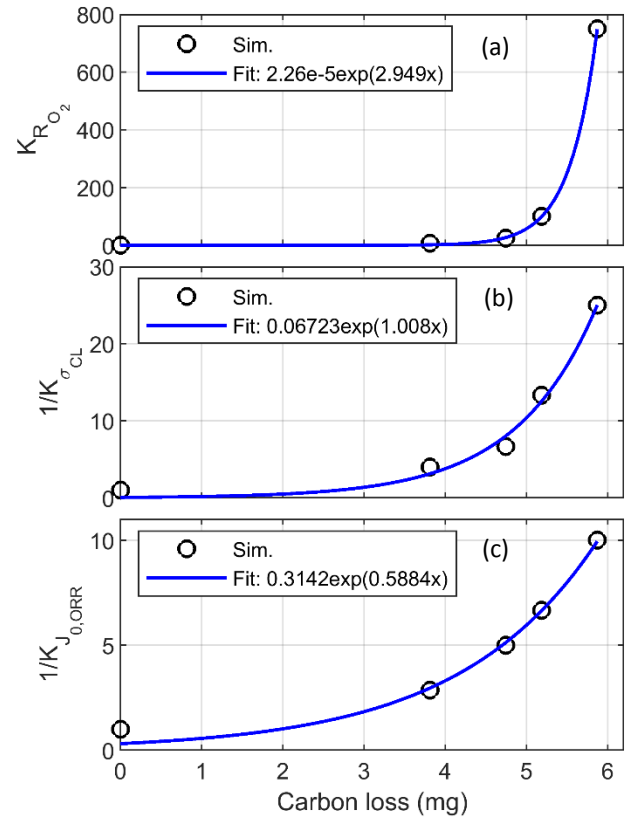


Fig 6 Variations of a) resistance of the CL against oxygen transport, b) proton conductivity of the CL, and c) exchange current density of ORR versus carbon loss of the CL; K is a coefficient that multiplies to these parameters for their variations

the effects of CL transport properties (resistance against oxygen transport, proton conductivity, and exchange current density of ORR) and agglomerate parameters (ionomer film thickness around the agglomerates and agglomerates radius) on the cell performance. It is found that thinner ionomer film, smaller agglomerates, higher exchange current density, lower transport resistance, and higher proton conductivity improve the cell performance. Transport parameters of the CL are varied to fit the polarization curves to the ones reported in [16] for an AST. Results demonstrate that transport parameters of the cathode CL change exponentially with carbon loss of the CL.

ACKNOWLEDGMENT

This work was supported by The Scientific and Technological Research Council of Turkey, TUBITAK-213M023.

REFERENCE

- [1] Pei P, Chang Q, Tang T. A quick evaluating method for automotive fuel cell lifetime. *International Journal of Hydrogen Energy*. 2008 Jul 1;33(14):3829-36.
- [2] Weber AZ, Borup RL, Darling RM, Das PK, Dursch TJ, Gu W, Harvey D, Kusoglu A, Litster S, Mench MM, Mukundan R. A critical review of modeling transport phenomena in polymer-electrolyte fuel cells. *Journal of The Electrochemical Society*. 2014 Jan 1;161(12):F1254-99.
- [3] Reiser CA, Bregoli L, Patterson TW, Jung SY, Yang JD, Perry ML, Jarvi TD. A reverse-current decay mechanism for fuel cells. *Electrochemical and Solid-State Letters*. 2005 Jun 1;8(6):A273-6.
- [4] Dubau L, Castanheira L, Maillard F, Chatenet M, Lottin O, Maranzana G, Dillet J, Lamibrac A, Perrin JC, Moukheiber E, Elkaddouri A. A review of PEM fuel cell durability: materials degradation, local heterogeneities of aging and possible mitigation strategies. *Wiley Interdisciplinary Reviews: Energy and Environment*. 2014 Nov;3(6):540-60.
- [5] Park JH, Yim SD, Kim T, Park SH, Yoon YG, Park GG, Yang TH, Park ED. Understanding the mechanism of membrane electrode assembly degradation by carbon corrosion by analyzing the microstructural changes in the cathode catalyst layers and polarization losses in proton exchange membrane fuel cell. *Electrochimica Acta*. 2012 Nov 30;83:294-304.
- [6] Lin R, Li B, Hou YP, Ma JM. Investigation of dynamic driving cycle effect on performance degradation and micro-structure change of PEM fuel cell. *International Journal of Hydrogen Energy*. 2009 Mar 1;34(5):2369-76.
- [7] Wang X, Kumar R, Myers DJ. Effect of voltage on platinum dissolution relevance to polymer electrolyte fuel cells. *Electrochemical and Solid-State Letters*. 2006 May 1;9(5):A225-7.
- [8] Ferreira PJ, Shao-Horn Y, Morgan D, Makharia R, Kocha S, Gasteiger HA. Instability of Pt / C electrocatalysts in proton exchange membrane fuel cells a mechanistic investigation. *Journal of The Electrochemical Society*. 2005 Nov 1;152(11):A2256-71.
- [9] Mitsushima S, Kawahara S, Ota KI, Kamiya N. Consumption rate of Pt under potential cycling. *Journal of The Electrochemical Society*. 2007 Feb 1;154(2):B153-8.
- [10] Zhang L, Shi W, Zhang B. A review of electrocatalyst characterization by transmission electron microscopy. *Journal of Energy Chemistry*. 2017 Nov 1;26(6):1117-35.
- [11] Ahluwalia RK, Arisetty S, Peng JK, Subbaraman R, Wang X, Kariuki N, Myers DJ, Mukundan R, Borup R, Plevaya O. Dynamics of particle growth and electrochemical surface area loss due to platinum dissolution. *Journal of The Electrochemical Society*. 2014 Jan 1;161(3):F291-304.
- [12] Chen J, Siegel JB, Matsuura T, Stefanopoulou AG. Carbon corrosion in PEM fuel cell dead-ended anode operations. *Journal of The Electrochemical Society*. 2011 Sep 1;158(9):B1164-74.
- [13] Kulikovskiy AA. Understanding catalyst layer degradation in PEM fuel cell through polarization curve fitting. *Electrocatalysis*. 2014 Jul 1;5(3):221-5.
- [14] Baroody HA, Stolar DB, Eikerling MH. Modelling-based data treatment and analytics of catalyst degradation in polymer electrolyte fuel cells. *Electrochimica Acta*. 2018 Sep 1;283:1006-16.
- [15] Dhanushkodi SR, Kundu S, Fowler MW, Pritzker MD. Use of mechanistic carbon corrosion model to predict performance loss in Polymer Electrolyte Membrane fuel cells. *Journal of Power Sources*. 2014 Dec 1;267:171-81.
- [16] Spornjak D, Fairweather J, Mukundan R, Rockward T, Borup RL. Influence of the microporous layer on carbon corrosion in the catalyst layer of a polymer electrolyte membrane fuel cell. *Journal of Power Sources*. 2012 Sep 15;214:386-98.
- [17] Rizvandi OB, Yesilyurt S. A pseudo three-dimensional, two-phase, non-isothermal model of proton exchange membrane fuel cell. *Electrochimica Acta*. 2019 Apr 10;302:180-97.
- [18] Karan K. PEFC catalyst layer: Recent advances in materials, microstructural characterization, and modeling. *Current Opinion in Electrochemistry*. 2017 Oct 1;5(1):27-35.
- [19] Carnes B, Spornjak D, Luo G, Hao L, Chen KS, Wang CY, Mukundan R, Borup RL. Validation of a two-phase multidimensional polymer electrolyte membrane fuel cell computational model using current distribution measurements. *Journal of Power Sources*. 2013 Aug 15;236:126-37.
- [20] Ye Q, Van Nguyen T. Three-dimensional simulation of liquid water distribution in a PEMFC with experimentally measured capillary functions. *Journal of the Electrochemical Society*. 2007 Dec 1;154(12):B1242-51.
- [21] Pokhrel A, El Hannach M, Orfino FP, Dutta M, Kjeang E. Failure analysis of fuel cell electrodes using three-dimensional multi-length scale X-ray computed tomography. *Journal of Power Sources*. 2016 Oct 15;329:330-8.